Applied Surface Science 593 (2022) 153363

Contents lists available at ScienceDirect

Applied Surface Science

journal homepage: www.elsevier.com/locate/apsusc

Full Length Article

Bond formation at polycarbonate | X interfaces (X = Ti, Al, TiAl) probed by X-ray photoelectron spectroscopy and density functional theory molecular dynamics simulations

Lena Patterer [*], Pavel Ondračka, Dimitri Bogdanovski, Leonie Jende, Stephan Prünte [1], Stanislav Mráz, Soheil Karimi Aghda, Bastian Stelzer, Markus Momma, Jochen M. Schneider

Materials Chemistry, RWTH Aachen University, Kopernikusstr. 10, 52074 Aachen, Germany

ARTICLE INFO

Keywords:
Polycarbonate
Sputter deposition
Interfacial bonding analysis
XPS
DFT
Molecular dynamics

ABSTRACT

To investigate the bond formation at polycarbonate (PC) | X interfaces (X = Ti, Al, TiAl) by X-ray photoelectron spectroscopy, thin metallic layers were deposited onto PC substrates by direct current magnetron sputtering. Additionally, changes in the chemical state of the polymer were studied systematically by density functional theory molecular dynamics simulations of a PC dimer interacting with the corresponding metallic surfaces. These predictions were confirmed by experiments, indicating a higher reactivity at PC | Ti interfaces: Ti reacts with all functional groups of PC, forming numerous interfacial C—Ti and (C—O)—Ti bonds, whereas Al exhibits selective reactivity as only (C—O)—Al bonds with the carbonate group are formed. However, integrated crystal orbital Hamilton population (ICOHP) calculations indicate a significantly higher interfacial bond strength for (C—O)—Al bonds compared to (C—O)—Ti and C—Ti bonds (ICOHP differences up to 3.1 eV). By multiplying the experimentally determined relative interfacial bond concentration with the theoretically determined maximum bond strength as an indicator for adhesion, the PC | Ti interface exhibits a ~1.9 and ~1.4 times larger value compared to the PC | Al and the PC | TiAl interface, respectively. Thus, Ti thin films are the preferential choice as adhesion layers for PC.

1. Introduction

Metalized polymers are utilized within microelectronics [1], food-packaging [2], aerospace [3], and automotive [4] industries. Sufficient adhesion of metal layers to polymer components is a key requirement for these applications. Examining the interfacial chemistry elucidates the reactivity between metal and individual functional groups of polymers, specifically regarding bond density and bond strength, which define adhesion.

Poly(bisphenol A carbonate), often referred to as polycarbonate (PC), is a thermoplastic polymer with widespread application in construction, automotive, and aerospace industries, in data storage, as well as for electrical and telecommunication hardware [5,6]. Ti and Al are elements employed in several technologically relevant coating materials ranging from metallic Al [7] to ceramic thin films, such as Al_2O_3 [8], TiN [9] as well as metastable cubic (Ti,Al)(O,N) [10]. Especially for these more complex functional thin films, metallic interlayers are employed to improve adhesion to polymer components [10,11].

Massaro et al. [12] investigated the interfacial bond formation between PC and evaporated Al by *in-situ* X-ray photoelectron spectroscopy (XPS). Several reaction stages were proposed: First, Al reacts with the carbonyl group (—C═O), and subsequently, Al reacts with the C_{ring}—O group. Both reactions result in the formation of (C—O)—Al bonds. These reactions were inferred from the observed decreasing signal of the carbonate as well as the C_{ring}—O group and the simultaneous appearance of an additional signal in the C 1s spectrum at a binding energy (BE) of 282.9 eV, which was attributed to (C—O)—Al bonds. After an Al layer thickness of 1.7 Å was reached, a second new component was observed at a BE = 280.6 eV, which was ascribed to the formation of C—Al bonds due to the reaction of Al with the aromatic group [12].

Abbreviations: AdC, adventitious carbon; BE, Binding energy; DFT, Density Functional Theory; ICOHP, integrated crystal orbital Hamilton population; MD, molecular dynamics; PC, polycarbonate; PET, polyethylene terephthalate; SAMs, self-assembled monolayers; XPS, X-ray photoelectron spectroscopy.

* Corresponding author.
E-mail address: patterer@mch.rwth-aachen.de (L. Patterer).
[1] Present address: Department of Applied Physics, Eindhoven University of Technology, Eindhoven 5600 MB, The Netherlands.

https://doi.org/10.1016/j.apsusc.2022.153363
Received 20 November 2021; Received in revised form 27 February 2022; Accepted 8 April 2022
Available online 15 April 2022

Consistent with these findings, interfacial studies of PC and evaporated Al carried out by Seidel et al. [13] and Rastomjee et al. [14] did report the formation of (C—O)—Al bonds, but in contrast to Massaro et al. [12], no evidence for the formation of C-Al bonds [13,14] was observed.

Relevant insights regarding the reactivity of Al with PC can also be obtained from reports delineating the interaction between Al and self-assembled monolayers (SAMs) which in terms of their termination are chemically identical [15,16] or similar [15–17] to PC functional groups or fragments thereof. These studies reported no interaction between Al and SAMs that consist of C—C or C—H groups [15–17]; however, chemical interactions of Al with C—O groups were identified by a combined XPS, infrared spectroscopy, and time-of-flight secondary ion mass spectrometry analysis [15–17]. Fisher et al. [16] performed quantum chemical calculations of the standard reaction enthalpies associated with the insertion of Al into various functional groups of PC: While Al insertions in C—C or C—H bonds are, in fact, energetically stable ($\Delta H^\circ = -82$ kJ/mol and $\Delta H^\circ = -44$ kJ/mol, respectively), the formation of O—Al—H and C—Al—OH bonds ($\Delta H^\circ = -188$ kJ/mol and $\Delta H^\circ = -248$ kJ/mol, respectively) appears to be even more likely. However, since no reaction between Al and hydrocarbon SAMs was observed in the experimental part of their correlative study, Fisher et al. [16] concluded that the formation of C-Al bonds is kinetically limited.

With regards to the PC | Ti interface, there is a lack of understanding about the interfacial bond formation in literature so far. Nevertheless, reports about the interaction between Ti and other polymers indicate the reaction of Ti with various functional groups, forming carbides [18–22], oxides [18,19,21], and nitrides [18] at polymer interfaces. Additionally, Konstadinidis et al. [23] investigated the interaction between evaporated Ti and differently terminated SAMs by XPS and sorted the relative reactivity of Ti towards different functional groups in the following order: —C═O> —C≡N> —COH> C—O—C> —CH_3.

Theoretical studies that do not focus on PC-containing interfaces may still be relevant if metals of interest interact with polymers containing similar functional groups as PC. For example, Calderone et al. [24] investigated the interaction between two Al atoms and a short molecular model system of polyethylene terephthalate (PET), which consists of aromatic and ester (—(C═O)—O—) groups. They determined that Al reacts preferentially with the ester group by forming covalent bonds with the O and C atoms of this group. Also, bonds between Al and the aromatic group were identified, but these organometallic bonds seem significantly less stable compared to (C—O)—Al bonds [24]. Similar to that, Chakraborty et al. [25] investigated the interaction between Al and acrylic polymers theoretically and determined that Al atoms interact exclusively with the carbonyl functional group (—C═O), whereas the methoxy groups (—O—CH_3) seemed unreactive towards the Al atoms. Recently, a complementary DFT and XPS study was published on the bond formation between Al and poly-epoxy, which is a polymer that also contains bisphenol A (a precursor monomer of PC) in its structure [26]. They simulated XPS spectra with respect to different adsorption sites for the metallic atoms at the organic molecule. From the comparison of the theoretical spectra with the experimentally obtained XPS spectra, conclusions about the interfacial bond formation were drawn, suggesting only the formation of (C—O)—Al bonds at the interface [26] which is consistent with Seidel et al. [13] and Rastomjee et al. [14] and in conflict with Massaro et al. [12].

These partly contradictory literature reports regarding the bond formation at the PC | Al interface together with the fact that the reactivity of the PC | Ti interface has not been investigated systematically motivated the here communicated research. Correlative theoretical and experimental investigations were carried out to study the interfacial bond formation between PC and Al, Ti, as well as TiAl layers systematically in order to design adhesion layers that maximize bond strength and bond density.

2. Methods

PC substrates were prepared by using a 5 wt% solution of PC pellets (additive-free, product # 4315139, Sigma-Aldrich) dissolved in tetrahydrofuran (anhydrous, 99.9% purity, inhibitor-free, Sigma-Aldrich) which was spin-coated (2000 rpm) on fused silica substrates (1×1 cm^2, Siegert Wafer). Immediately after preparation, the substrates were inserted into the deposition chamber to minimize surface contamination due to adventitious carbon (AdC).

Metallic thin films were synthesized by direct current magnetron sputtering in a laboratory-scale deposition system described elsewhere [27]. 99.995% pure Ti, 99.99% pure Al, and 99.99% pure $Ti_{0.5}Al_{0.5}$ targets (Ø 50 mm) were placed at a target-to-substrate distance of 10 cm. The substrate holder was kept at floating potential and was rotated during depositions with a speed of 28 rpm to ensure a homogenous deposition. The employed target power density was kept constant at 10.2 W cm^{-2} for all three metallic depositions. All depositions were performed without intentional heating and at a base pressure $\leq 2 \times 10^{-4}$ Pa. Argon (6.0 purity) was used as the sputtering gas at a working pressure of 0.5 Pa for Al and Ti depositions. To achieve the atomic ratio of Al/Ti ~ 1 for the TiAl thin film, a working pressure of 1 Pa was employed. Prior to each deposition, sputter cleaning was performed for ~5 min behind a closed shutter to clean the target surface.

To determine the film thickness and the consequent deposition rate of the metallic thin films, cross-sections were analyzed using a FEI Helios Nanolab 660 equipped with a field-emission microscope. The acceleration voltage and the current were set to 10 kV and 50 pA, respectively. For the experimental PC | X interfaces (X = Ti, Al, TiAl), a metal layer thickness <1 nm was chosen to ensure that the total volume probed by XPS contains the interface between the metallic layer and PC. Therefore, deposition time and respective layer thickness d according to Table 1 were chosen to ensure comparable conditions regarding interface formation.

After deposition, the samples were immediately transferred to the XPS analysis chamber with an atmosphere exposure time <5 min. The interfacial bond formation and the chemical composition were analyzed by XPS using an AXIS SUPRA (Kratos Analytical Ltd.), equipped with a monochromatic Al-K_α X-ray source and a hemispherical detector. During spectra acquisition, the base pressure of the system was $<5.0 \times 10^{-6}$ Pa. For chemical analysis, survey scans with a pass energy of 160 eV and a step size of 0.25 eV were performed (5 sweeps, dwell time of 100 ms). High-resolution C 1s XPS spectra were obtained using a pass energy of 20 eV and a step size of 0.05 eV (20 sweeps, dwell time of 100 ms). During acquisition, a charge neutralizer (low-energy, electron-only source) was used to avoid charging effects. The spectra were analyzed and fitted using the CasaXPS software package (Casa Software Ltd.). The chemical analysis was performed by applying the respective sensitivity factors provided by the manufacturer of the XPS system. XPS data fitting of the high-resolution spectra was performed using a mixed Gaussian-Lorentzian (70%–30%) peak shape and the subtraction of a Shirley background. The interfacial XPS analysis focuses on the C 1s signal, as the O 1s, Al 2p, and Ti 2p signals are affected by both interfacial reactions and surface oxidation. The full width at half maximum of the fitted C 1s components was constrained to be below 1.5 eV. Even though the aliphatic and aromatic contributions exhibit only a ΔBE of 0.5 eV, they were fitted individually for pristine PC due to their known area ratio of 1/3 [28]. For the metalized PC samples, however, it is unknown how the ratio of aliphatic and aromatic contributions is affected by the

Table 1
Deposition rate, time, and thickness for the synthesis of Ti, Al, and TiAl layers.

	Deposition rate [nm/min]	Deposition time [s]	d [nm]
Ti	18	3	0.9
Al	33	1	0.6
TiAl	20	2	0.7

interface reactions or by particle bombardment during sputtering. Therefore, the aliphatic and aromatic contributions were combined as one component for the interface analysis. The BE scale was calibrated to the aromatic component at 284.5 eV for pristine PC [28], whereas the combined aliphatic + aromatic component was set to 284.6 eV for the metalized samples [29].

Density Functional Theory (DFT) [30,31] as implemented in the OpenMX package [32–35] was employed to model the PC-surface interaction and calculate the C 1s BEs. Since the experimental structure of the 2 monolayer thick metal films is unknown at the interface, the simplest surfaces were chosen for the simulation, namely the hexagonal close-packed α-Ti(0001), the tetragonal γ-TiAl(100), and the face-centered cubic Al(100) surface. A PC dimer was placed at a distance of 5 Å from the surfaces, and an *ab initio* molecular dynamics (MD) run was initiated with the temperature set to 500 K and 600 K. Especially for the bond strength analysis, the presence of metallic layers following the interface is considered to yield a more realistic description of the interfacial bond formation compared to single metal atoms being bonded to a polymer. While the PC dimer was attracted by the Ti and TiAl surface and reacted eventually, the PC | Al system needed an additional impulse for the interface reaction to occur within the time-scales of the MD run. After an initial thermalization period, the PC dimer was provided with an initial velocity of 2000 m/s (corresponding to ~0.25 eV for a C atom) in the direction of the Al surface.

The MD simulations were conducted until significant interactions with the metallic surfaces could be observed which often ended in a decomposition of the PC dimer. The temperature was controlled with the Nosé-Hoover [36] thermostat and the MD simulation time step was set to 0.5 fs. Afterwards, representative configurations of functional groups interacting with the metal surfaces at 500 K were selected for the subsequent analysis. The configurations were relaxed such that the residual forces were less than 0.16 eV/Å to reduce the influence of the atomic vibrations on the calculated BEs and the C 1s core-electron binding energies were calculated for all C atoms using the method of Ozaki [37]. For the purpose of visual comparison with experimental spectra, a Gaussian broadening with a stand deviation of $\sigma = 0.3$ eV was applied to the calculated discrete BEs. Simulations at 600 K were carried out to study the interfacial bond formation events under more reactive boundary conditions. A standard precision basis set was used for the MD and force relaxation (H6.0-s2p1, C6.0-s2p2d1, O6.0-s2p2d1, Ti7.0-s3p2d1), while an improved precision basis including the 1 s states was used for the C and O atoms for the BE calculations (C7.0_1s-s4p3d2, O7.0_1s-s4p3d2). Energy cutoffs of 300 Ry were used for MD and relaxation steps, and 400 Ry for the calculation of the BEs. A dispersion correction was applied with the DFT-D3 approach [38].

Selected configurations obtained from the preceding *ab initio* MD runs were used as starting points for static DFT calculations utilizing the Vienna *ab initio* Simulation Package (VASP, version 5.4.4.) [39–41] employing projector-augmented wave basis sets [42] with cut-off energies of 500 eV and a Gaussian smearing to consider electronic occupation. Both VASP and OpenMX runs modeled the electron exchange and correlation effects *via* the well-established Perdew-Burke-Ernzerhof (PBE) parametrization [43] of the generalized gradient approximation and the Brillouin zone was sampled at the Γ-point only due to the large system sizes (several hundred atoms in each case).

Bonding analysis was performed *via* calculation of the crystal orbital Hamilton populations (COHP) [44] from the VASP wave functions *via* the LOBSTER package (version 4.0.0) [45–47]. The optimized PBE-VaspFit2015 basis set [48] was used for local orbital reconstruction, with basis functions corresponding to the choice of the PAW potentials in respect to valence electron configuration: $3s^2 3p^1$ for Al, $4s^1 3d^3$ for Ti, $2s^2 2p^4$ for O, $2s^2 2p^2$ for C, and $1s^1$ for H. After projection and calculation of the COHP, the integrated values (ICOHP) per bond were extracted and interpreted as an indirect, but strongly correlated indicator of bond strength.

All calculations data with further details are available in the NOMAD Archive [49].

3. Results and discussion

Representative MD configurations of the PC | X interfaces (X = Ti, Al, TiAl) at 500 and 600 K are shown in Table 2. Generally, it is predicted that the PC dimer reacts with Ti and TiAl surfaces by forming interfacial bonds mediated by the decomposition of aromatic and carbonate groups (Table 2 a & c). At 600 K, the formation of interfacial bonds between aliphatic fragments and Ti can be observed as well (Table 2 a). In contrast, the PC dimer reacts with the Al surface only by forming bonds with the decomposing carbonate group (Table 2 b). Due to a rather repulsive force between the hydrocarbon groups and the Al surface, Al atoms bonded to the carbonate group are pulled out of the Al crystal (Table 2 b, 500 and 600 K).

In the following, the theoretically calculated broadened BEs and experimentally measured XPS spectra are compared for pristine PC (Fig. 1), as well as the PC | Ti (Fig. 2, Fig. 3), PC | Al (Fig. 5, Fig. 6), and PC | TiAl (Fig. 7, Fig. 8) interfaces. In Fig. 2, Fig. 5, and Fig. 7, the simulated broadened BEs of a pristine PC dimer (a), as well as of two different MD configurations (b & c) are shown, enabling the identification of differences and similarities regarding the bond formation between the studied interfaces. The BEs of the components attributed to interfacial bonds determined theoretically and experimentally are shown in Table 3 and Table 4, respectively.

The BEs determined theoretically for a PC dimer (dashed line) and experimentally for a spin-coated PC sample (solid line) are shown in Fig. 1. For both, the BE scale was calibrated with respect to the aromatic component to 284.5 eV [28]. Besides the aromatic group, the experimentally obtained XPS spectrum contains components attributed to the aliphatic group at 285.0 eV, the C_{ring}—O group at 286.1 eV, and the carbonate group (O—(C═O)—O) at 290.5 eV which is in good agreement with literature [28,29,51], also regarding the C 1s signals of two π-π* shakeup satellites (291.4 eV, 292.6 eV) [29]. Additionally, the C/O ratio of pristine PC determined by XPS (85 at.% C and 15 at.% O) is in good agreement with literature values [29].

By comparing the measured with the calculated BEs of the functional groups, very good agreement is evident (Figure 1). However, it can be seen that the absolute value for the ΔBE of the carbonate group with respect to the aromatic group is slightly underestimated by DFT. Nevertheless, the trend of chemical shifts within the theoretical BEs is consistent with the experimental spectrum, rendering the prediction of BE shifts by DFT with the here employed methodology as sound.

From MD simulations of the PC | Ti interface, it is predicted that reactions of the PC dimer with the Ti surface are initiated by both the carbonate as well the aromatic groups (Fig. 2 b). As shown in Fig. 2 a & b, initially, the theoretically determined BEs of both groups (Fig. 2 a) are shifted towards lower values, indicating the formation of (C—O)—Ti (red component, Fig. 2 b) and C—Ti bonds (green component, Fig. 2 b), respectively. Continuing the MD run, the PC dimer decomposes at the carbonate group into two fragments (Fig. 2 c). The component attributed to (C—O)—Ti bonds is then shifted to even lower BEs and overlaps with the C_{ring}—O component (Fig. 2 c).

In Fig. 3 b, consistent with the DFT predictions (Fig. 2 b), the formation of (C—O)—Ti and C—Ti bonds is experimentally evident, since new components at BE = 289.2 eV and at BE = 282.0 eV are observed, respectively. Additionally, a second (C—O)—Ti component was fitted at BE = 285.8 eV since this component, caused by the reaction of Ti with

Table 2
Representative MD configurations for the PC dimer interacting with a) Ti, b) Al, and c) TiAl surfaces at 500 and 600 K [50].

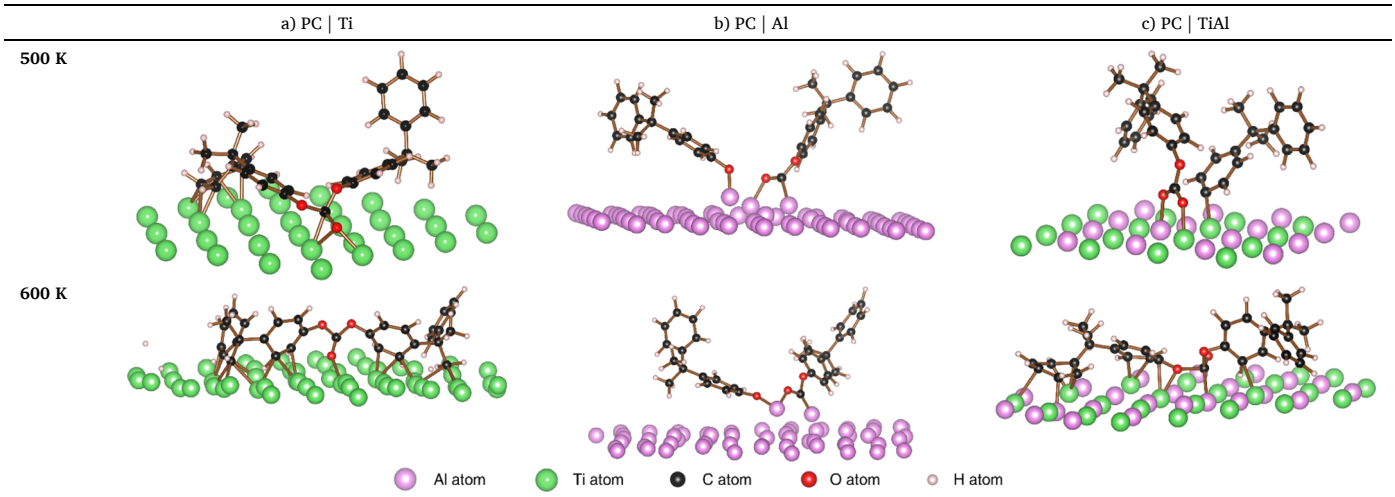

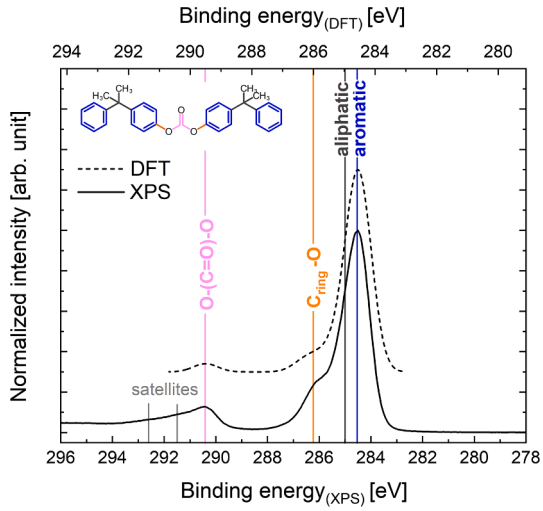

Fig. 1. C 1s spectrum determined by XPS (lower x-axis) and broadened BEs calculated by DFT (upper x-axis) for pristine PC (functional groups are indicated by colored lines).

the decomposed carbonate group, is predicted by the MD simulation (Fig. 2 c). In line with this, the components attributed to the carbonate group as well as of the π-π* shakeup satellites are decreased compared to pristine PC (Fig. 3 a & b), indicating reactions at the carbonate and the aromatic groups, respectively [12,13,52].

Since the (C—O)—Ti components represent reaction products with the carbonate and the C_{ring}—O group, the area fractions of the O—(C═O)—O + C_{ring}—O + both (C—O)—Ti components for the experimental PC | Ti interface should be in the same range compared to the area fractions of the C_{ring}—O + O—(C═O)—O components for pristine PC. However, for the experimental PC | Ti interface, a decrease for these area fractions compared to pristine PC (from 25 to 18%, see supplementary information, **Table S1**) was observed, indicating TiO_x formation at the interface which cannot be quantified from the C 1s signal [18].

The aforementioned C—Ti signal was assumed to be due to interface reactions but could also be caused by reactions with carbon-containing residual gases. To identify the origin of the C—Ti signal, a ~720 nm thick Ti film was grown and analyzed by XPS. In contrast to the thin Ti film - employed throughout this paper for interface analysis, no C—Ti signal was observed for the thick Ti film (see supplementary information, Fig. S1). Therefore, it is evident that the C—Ti signal is, in fact, caused by chemical reactions at the interface between Ti and PC rather than by a surface reaction with residual gas.

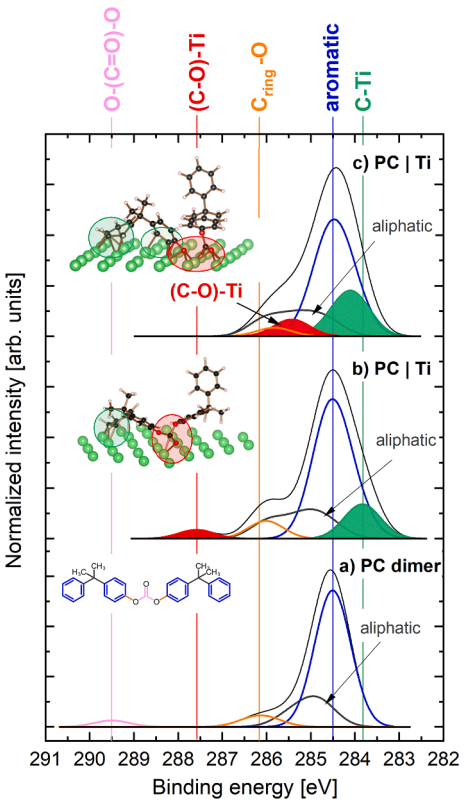

Fig. 2. C 1s broadened BEs obtained by DFT for a) the pristine PC dimer and b) & c) the PC | Ti interface for different MD configurations.

Similar to the PC | Ti interface, the MD simulations for the PC | Al interface predict the formation of (C—O)—Al bonds with a negative BE shift relative to the pristine carbonate group (Fig. 5). However, in contrast to the PC | Ti interface, the PC dimer immediately decomposes into two fragments upon initial interaction with the Al surface. The immediate configuration before the decomposition at the carbonate group is represented by the configuration shown in Fig. 5 b and Fig. 4 a, where the carbonate group is still intact. However, from bond strength

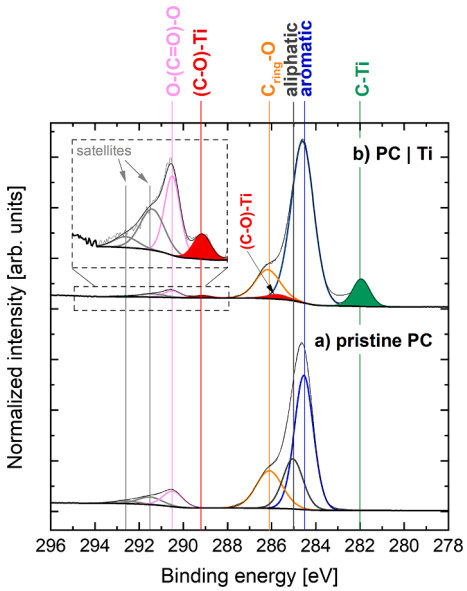

Fig. 3. XPS C 1s spectra for a) pristine PC and b) the PC | Ti interface (magnification of interface signal at BE = 288–295 eV); for the interface, the aromatic and aliphatic components are combined to one hydrocarbon component since their ratio change after deposition is unknown and hence, cannot be resolved.

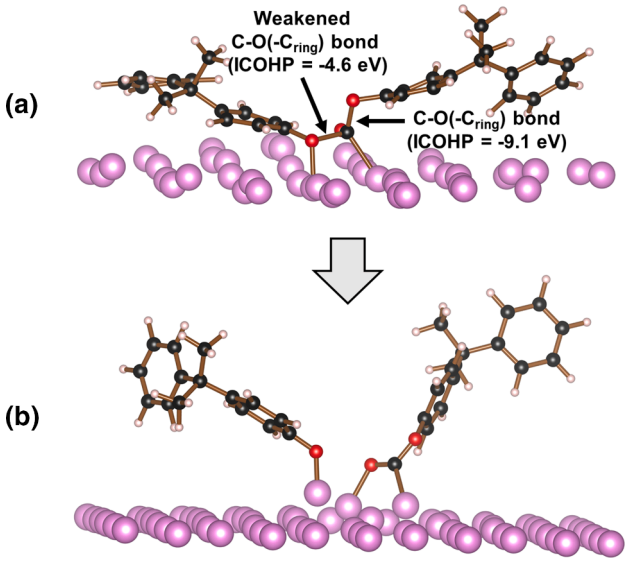

Fig. 4. MD configuration of the PC | Al interface upon a) the initial interaction (with ICOHP values) and b) advanced interaction.

(ICOHP) analysis (Fig. 4 a), it is observed that the bridging C—O(—C$_{ring}$) bond (Fig. 5 b) that is to be broken upon continuing the simulation (Fig. 4 b and Fig. 5 c) exhibits only half of the bond strength (−4.6 eV) compared to the bridging C—O(—C$_{ring}$) bond which stays intact (−9.1 eV).

This indicates interaction-induced bond weakening for the MD configuration in Fig. 5 b which results in a subsequent decomposition into two fragments (Fig. 5 c). Consequently, relative to the pristine carbonate group, the component attributed to (C—O)—Al bonds shown in Fig. 5 b exhibit a higher ΔBE (2.9 eV) compared to the (C—O)—Ti component (1.9 eV, Fig. 2 b), (Table 3). The respective experimental component, indicating interfacial (C—O)—Al bonds, is displayed at BE = 289.6 eV (blue component, Fig. 6 b).

After the PC dimer decomposes into two fragments, both react with

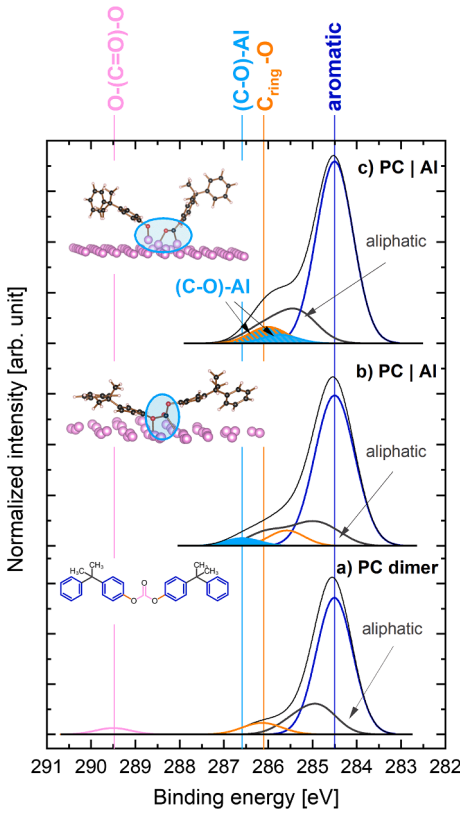

Fig. 5. C 1s broadened BEs obtained by DFT for a) the pristine PC dimer and b) & c) the PC | Al interface for different MD configurations.

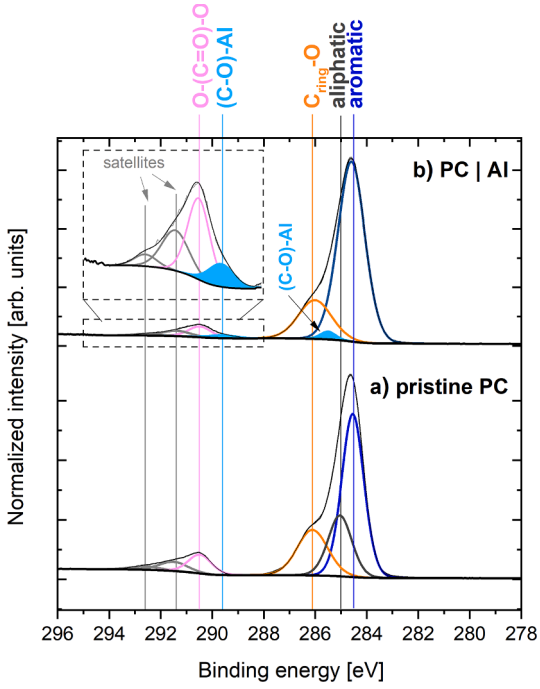

Fig. 6. XPS C 1s spectra for a) pristine PC and b) the PC | Al interface (magnification of interface signal at BE = 288–295 eV); for the interface, the aromatic and aliphatic components are combined to one hydrocarbon component since their ratio change after deposition is unknown and hence, cannot be resolved.

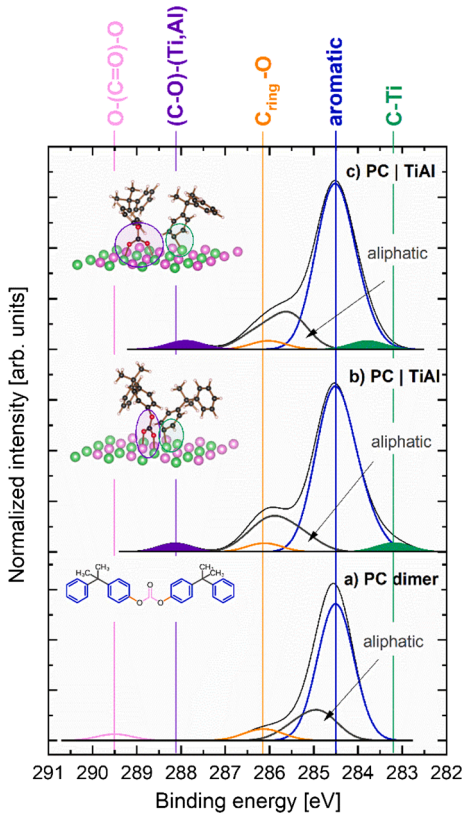

Fig. 7. C 1s broadened BEs obtained by DFT for a) the pristine PC dimer and b) & c) the PC | TiAl interface for different MD configurations.

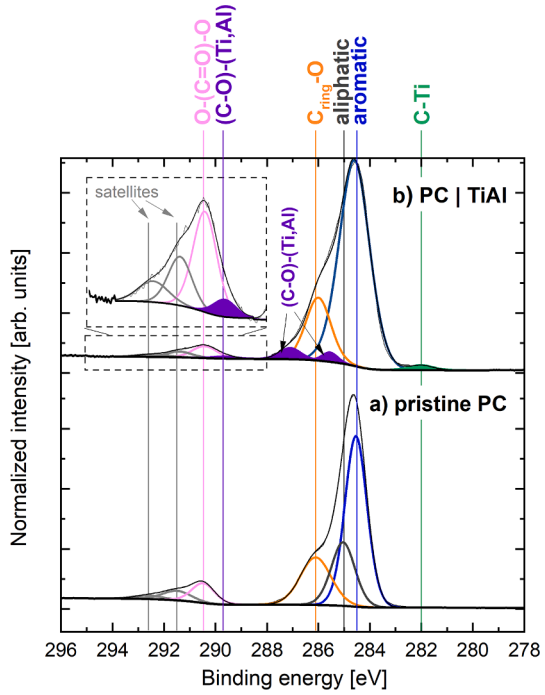

Fig. 8. XPS C 1s spectra for a) pristine PC and b) the PC | TiAl interface (magnification of interface signal at BE = 288–295 eV); for the interface, the aromatic and aliphatic components are combined to one hydrocarbon component since their ratio change after deposition is unknown and hence, cannot be resolved.

the Al surface forming two (C—O)—Al bonds (Fig. 5 c). These signals overlap in the theoretically determined BEs with the C_{ring}—O component at 286.0 eV (Fig. 5 c) and in the experimental spectrum, these bonds are indicated by a component at BE = 285.5 eV (Fig. 6 b).

Here, the formation of interfacial C—Al bonds caused by a reaction between Al and hydrocarbon groups of PC, as it was observed by Massaro et al. [12], is neither observed in the simulations nor the experimental XPS data. This apparent contradiction may be rationalized by the fact that the here employed deposition rate of 33 nm/min is 100 times larger than the rate utilized in the Al evaporation study onto PC [12] and that the most probable kinetic energy of the deposited flux is in the order of eV rather than meV as during evaporation [53]. During vapor phase condensation, the phase formation – particularly of metastable phases – is well known to be deposition rate as well as kinetic energy dependent [54].

The MD simulation for the PC | TiAl interface predicts interfacial bond formation between the carbonate group and Ti as well as Al atoms to form (C—O)—(Ti,Al) bonds (indicated by the purple component at BE = 288.1 eV, Fig. 7 b). The continued simulation (Fig. 7 c) predicts higher tendencies to form (C—O)—(Ti,Ti) bonds, shifting the purple component to a BE = 287.9 eV. Experimentally, (C—O)—(Ti,Al) bonds are indicated by the component at 289.7 eV (Fig. 8 b). Furthermore, MD simulations predict interactions of the aromatic group exclusively with Ti surface atoms, forming a C—Ti bond with a negative BE shift relative to the C 1s signal of the aromatic group (green component, Fig. 7 b & c), which is consistent with a new component resolved experimentally at 282.0 eV (Fig. 8 b). Similar to the DFT predicted PC | Ti and PC | Al interfaces, two more (C—O)—(Ti,Al) components could be resolved at BE = 285.5 and 287.1 eV, indicating reactions of Ti and Al atoms with decomposed carbonate groups. DFT predictions showed that the electronic structure of (C—O)—Al and (C—O)—Ti components is characterized by several BEs (see Table 3), so that the component at 287.1 eV is assigned to a (third) type of (C—O)—(Ti,Al) bonds.

Overall, it can be seen that the simulated interface reactions are in very good agreement with the experimental data and, hence, enable bond formation predictions at interfaces.

By correlative analysis of the discussed theoretically and experimentally obtained BEs for components of pristine PC as well as of the PC | Ti, PC | Al, and PC | TiAl interfaces, it is evident that both the type and population of interfacial bonds formed depend strongly on the metal species.

For the experimental PC | Al and PC | TiAl interfaces, >75% of the changes in the C 1s signal compared to pristine PC (Fig. 9 a) can be assigned to interfacial (C—O)—Al and (C—O)—(Ti,Al) bonds, respectively (Fig. 9 b & c). In contrast, >70% of all experimentally detected interfacial components can be assigned to C—Ti bonds for the PC | Ti interface (Fig. 9 d).

In addition to the bond type ratios, information pertaining to the population of the interfacial bonds can be extracted from the ratio of interfacial components relative to the C 1s signal (Fig. 10). The diagram shows that the fraction of components, indicating interfacial (C—O)—Al, (C—O)—(Ti,Al), and (C—O)—Ti bonds, is similar for all three systems (3–4.8%). However, the component indicating C—Ti bonds at the PC | Ti interface is by far the largest (8.9%). Depositions with a longer deposition time even indicate that the amount of C—Ti bonds continues to increase, whereas the interfacial bond formation with the carbonate groups seems to be saturated (see supplementary information, **Fig. S2**). Hence, the PC | Ti interface exhibits ~4 times more interfacial bonds compared to the PC | Al interface, while at the PC | TiAl interface, ~2 times more interfacial bonds compared to the PC | Al interface are formed. Interestingly, the PC | TiAl interface exhibits only 15% of the C—Ti portion determined for the PC | Ti interface, even though it contains 50% Ti atoms. Hence, it is inferred that Al inhibits the formation of C—Ti bonds. This notion can be rationalized based on the PC | Al simulations, where it was observed that the hydrocarbon groups are repelled by Al, thereby resulting in an - based on the Ti population on the

Table 3
BEs of components indicating interfacial bonds determined by DFT for different MD configurations.

Interfacial bond	Interfaces	BE_{DFT} [eV]	$\lvert\Delta_{carbonate}BE_{DFT}\rvert$ [eV] ($BE_{carbonate}$ = 289.5 eV)	$\lvert\Delta_{aromatic}BE_{DFT}\rvert$ [eV] ($BE_{aromatic}$ = 284.5 eV)
(C-O)-Ti	PC_{intact} | Ti (Fig. 2 b)	287.6	1.9	--
(C-O)-Ti	$PC_{decomposed}$ | Ti (Fig. 2 c)	285.4	4.1	--
(C-O)-Al	PC_{intact} | Al (Fig. 5 b)	286.6	2.9	--
(C-O)-Al	$PC_{decomposed}$ | Al (Fig. 5 c)	286.0	3.5	--
(C-O)-(Ti,Al)	$PC_{decomposed}$ | TiAl (Fig. 7 b)	288.1	1.4	--
(C-O)-(Ti,Ti)	$PC_{decomposed}$ | TiAl (Fig. 7 c)	287.9	1.6	--
C-Ti	PC_{intact} | Ti (Fig. 2 b)	283.8	--	0.7
C-Ti	$PC_{decomposed}$ | Ti (Fig. 2 c)	284.0	--	0.5
C-Ti	$PC_{decomposed}$ | TiAl (Fig. 7 b)	283.2	--	1.3
C-Ti	$PC_{decomposed}$ | TiAl(Fig. 7 c)	283.8	--	0.7

Table 4
BEs of components indicating interfacial bonds determined by XPS.

Interfacial bond	Interfaces	BE_{XPS} [eV]	$\lvert\Delta_{carbonate}BE_{XPS}\rvert$ [eV] ($BE_{carbonate}$ = 290.5 eV)	$\lvert\Delta_{aromatic}BE_{XPS}\rvert$ [eV] ($BE_{aromatic}$ = 284.5 eV)
(C-O)-Ti	PC_{intact} | Ti (Fig. 3 b)	289.2	1.3	--
(C-O)-Ti	$PC_{decomposed}$ | Ti (Fig. 3 b)	285.8	4.7	--
(C-O)-Al	PC_{intact} | Al (Fig. 6 b)	289.6	0.9	--
(C-O)-Al	$PC_{decomposed}$ | Al (Fig. 6 b)	285.5	5.0	--
(C-O)-(Ti,Al)	PC_{intact} | TiAl (Fig. 8 b)	289.7	0.8	--
(C-O)-(Ti,Al)	$PC_{decomposed}$ | TiAl (Fig. 8 b)	285.5	5.0	--
(C-O)-(Ti,Al)	$PC_{decomposed}$ | TiAl (Fig. 8 b)	287.1	3.4	--
C-Ti	PC | Ti (Fig. 3 b)	282.0	--	2.5
C-Ti	PC | TiAl (Fig. 8 b)	282.0	--	2.5

surface - unexpectedly low population of the C—Ti bonds at the PC | TiAl interface.

Since the bond strength of interfacial bonds affects the adhesion, ICOHP calculations for different MD configurations are analyzed. In total, four different configurations were considered: One for the PC | Ti interface shown in Fig. 2 b, one for the PC | TiAl interface shown in Fig. 7 b, and two for the PC | Al interface shown in Fig. 5 b & c. For the PC | Al interface, two configurations were analyzed to have a similar ICOHP data set compared to the numerous Ti-based interfacial bonds. Accordingly, seven ICOHP values were obtained for interfacial C—Ti bonds, four ICOHP values for interfacial (C—O)—Ti bonds, and six ICOHP values for interfacial (C—O)—Al bonds (more details about the individual bonds can be found in the supplementary information). The overall results of this analysis are summarized in Fig. 11, showing the range of ICOHP values for the different interfacial bonds. Additionally, the graph shows the lower and the upper limit of the interatomic distances *r*. It must be noted that a more negative ICOHP value, and thus a larger absolute value signifies a stronger bond.

The distribution of interatomic distances indicates bond strength variations (Fig. 11): as a rule, with a shorter distance, the bond strength is increased. However, overall, it can be observed that the bond strength is mainly determined by the local chemical environment of the interface. Interfacial C—Ti bonds, formed by reactions between Ti atoms and the aromatic groups, exhibit ICOHP values in the range of −1.0 to −2.6 eV per bond (per bond is implied in the following), while the interfacial (C—O)—Ti bonds, formed by reactions between Ti and the carbonate groups, are characterized by ICOHP values between −1.5 and −2.6 eV. In contrast, the interfacial (C—O)—Al bonds, representing the bond formation between Al atoms and the carbonate group, exhibit ICOHP values between −2.8 and −5.7 eV, whereby a weaker bond strength is observed at the onset of interface formation (Fig. 5 b) and stronger bonds are formed as the interaction progresses (Fig. 5 c).

Both, the DFT binding analysis and the ICOHP analysis show no considerable interaction between Al atoms and hydrocarbon groups of PC. Instead, Al forms only bonds with the C atom from the carbonate group as the O atoms seem to play a mediating role, leading to interfacial

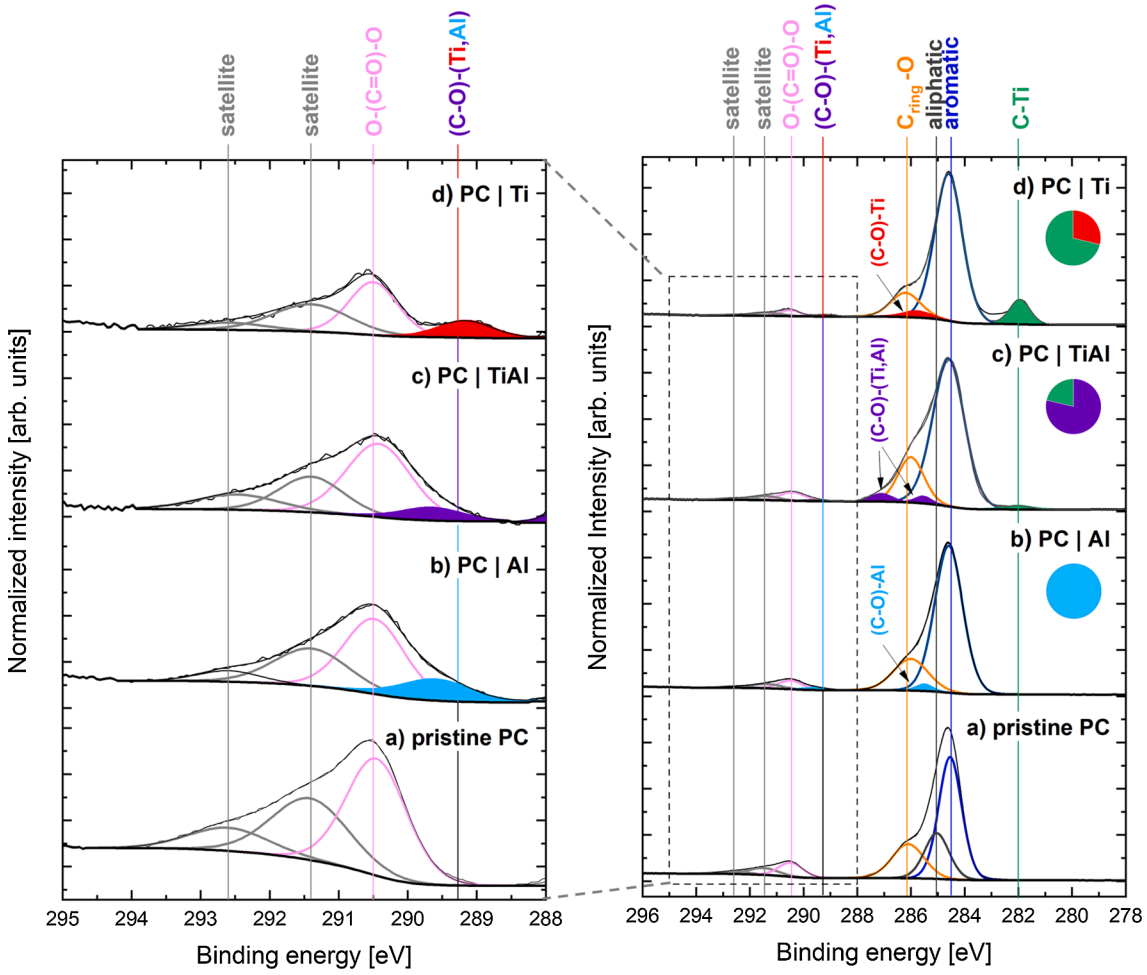

Fig. 9. C 1s spectra of PC | X interfaces (X = Al (b), TiAl (c), Ti (d)) in comparison to pristine PC (a) determined by XPS (interfacial bond ratios are indicated by pie charts color-coded according to the labels).

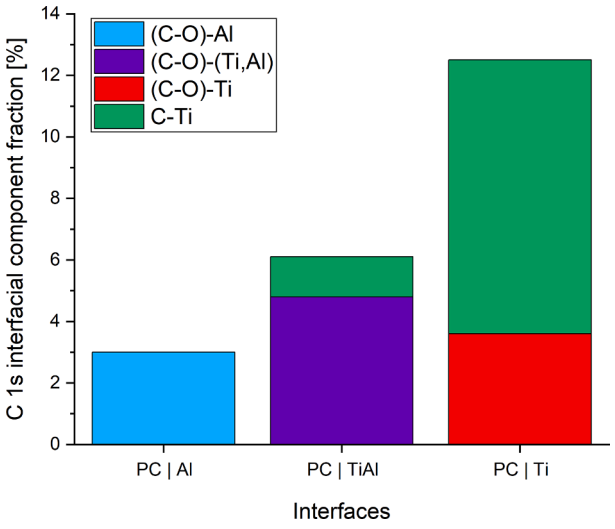

Fig. 10. Fraction of C 1s components corresponding to the interfacial bonds forming at PC | X interfaces (X = Al, TiAl, Ti) determined by XPS.

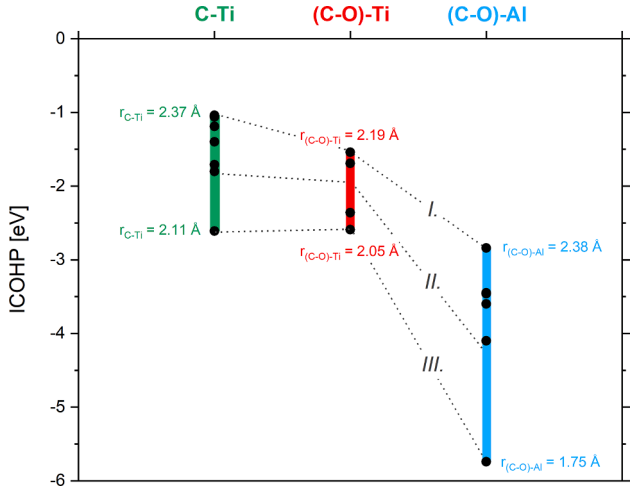

Fig. 11. Range of determined ICOHP values and interatomic distances (r) of interfacial bonds determined for different MD configurations.

(C—O)—Al bonds as it was already observed in other interface studies [15–17].

Since the most negative ICOHP values seem to represent the interface conditions after more advanced interaction, these values are used to compare the adhesion properties at the interfaces with each other in the further analysis of this study (Fig. 11, III.). From this data, it can be concluded that interfacial (C—O)—Al bonds potentially exhibit a significantly higher bond strength (ICOHP down to −5.7 eV) compared to interfacial C—Ti and (C—O)—Ti bonds (ICOHP for both only down to

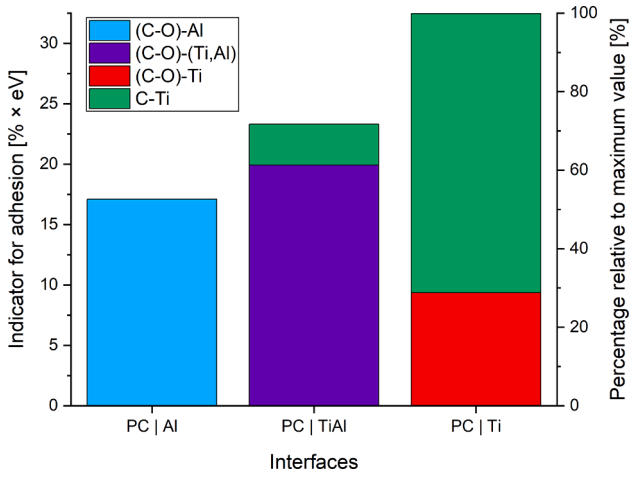

Fig. 12. Product of relative interfacial component concentration (XPS) and maximum determined interfacial bond strength (ICOHP) merged as an indicator for adhesion to compare PC | X interfaces (X = Al, TiAl, Ti).

−2.6 eV). This trend is also observed for the least negative and the average ICOHP values (Fig. 11, I. and II., respectively).

To evaluate the adhesion properties, quantitative XPS results, pertaining to bond population, and qualitative ICOHP values, closely correlated with bond strength, were merged in an indicator for adhesion: The relative interfacial bond concentration is multiplied by the highest determined absolute ICOHP value for the respective bond species to compare the three interfaces (Fig. 12).

It can be seen that the PC | Ti interface exhibits a ~1.9 times larger value compared to the PC | Al interface. For the ICOHP analysis of the PC | TiAl interface, a fraction of 50% (C—O)—Ti and 50% (C—O)—Al bonds is assumed for the (C—O)—(Ti,Al) component. In total, a ~1.4 times larger value for the PC | Ti interface compared to the PC | TiAl interface is determined (Fig. 12). From this data, we predict that the PC | Ti interface likely exhibits superior adhesion compared to average PC | TiAl and PC | Al interfaces.

4. Conclusions

The bond formation at PC | X interfaces (X = Ti, Al, TiAl) was systematically investigated by XPS as well as by DFT-MD simulations of a PC dimer interacting with the corresponding metallic surfaces. Comparing experimental data with predictions, irrefutable evidence is presented that interfacial bond formation can be predicted by the computational strategy employed here. Specifically, for the Ti, Al, and TiAl system, it is evident that most interfacial bonds are formed at the PC | Ti interface, namely (C—O)—Ti and C—Ti bonds. While for the Al system, no evidence for the formation of interfacial C—Al bonds could be obtained, (C—O)—Al bonds are formed instead. XPS investigations suggest a factor ~4 larger population of interfacial bonds at the PC | Ti interface compared to the PC | Al interface. However, ICOHP analyses performed to probe the interfacial bond strength show that (C—O)—Al bonds are significantly stronger than (C—O)—Ti and C—Ti bonds (ICOHP differences up to 3.1 eV). As both interfacial bond strength and the bond density affect adhesion, the relative interfacial bond concentration determined by XPS was multiplied by the theoretically determined maximum absolute ICOHP value, serving as an indicator for adhesion. Based on this assessment, the PC | Ti interface exhibits a ~1.9 times larger value than the PC | Al interface and a ~1.4 times larger value than the PC | TiAl interface. Hence, Ti is predicted to be the best choice of an adhesion layer for PC substrates compared to Al and TiAl.

CRediT authorship contribution statement

Lena Patterer: Conceptualization, Methodology, Formal analysis, Investigation, Writing – original draft, Visualization. **Pavel Ondračka:** Methodology, Formal analysis, Investigation, Writing – original draft. **Dimitri Bogdanovski:** Methodology, Formal analysis, Investigation, Writing – original draft. **Leonie Jende:** Formal analysis, Investigation, Writing – review & editing. **Stephan Prünte:** Formal analysis, Investigation, Writing – review & editing. **Stanislav Mráz:** Investigation, Writing – review & editing. **Soheil Karimi Aghda:** Formal analysis, Investigation, Writing – review & editing. **Bastian Stelzer:** Investigation, Writing – review & editing. **Markus Momma:** Investigation, Writing – review & editing. **Jochen M. Schneider:** Conceptualization, Methodology, Writing – original draft, Supervision, Project administration, Funding acquisition.

Declaration of Competing Interest

The authors declare that they have no known competing financial interests or personal relationships that could have appeared to influence the work reported in this paper.

Acknowledgment

This research was funded by the German Research Foundation (DFG, SFB-TR 87/3) “Pulsed high power plasmas for the synthesis of nanostructured functional layers”. The authors gratefully acknowledge the computing time granted by the JARA Vergabegremium and provided on the JARA Partition part of the supercomputer CLAIX at RWTH Aachen University (projects JARA0151 and JARA0221).

Appendix A. Supplementary material

Supplementary data to this article can be found online at https://doi.org/10.1016/j.apsusc.2022.153363.

References

[1] F. Faupel, V. Zaporojtchenko, T. Strunskus, J. Erichsen, K. Dolgner, A. Thran, M. Kiene, Fundamental Aspects of Polymer Metallization, in: E. Sacher (Ed.), Metallization of Polymers 2, Springer, US, Boston, MA, 2002, pp. 73–96.
[2] M. Ozdemir, C.U. Yurteri, H. Sadikoglu, Physical polymer surface modification methods and applications in food packaging polymers, Crit. Rev. Food Sci. Nutr. 39 (5) (1999) 457–477, https://doi.org/10.1080/10408699991279240.
[3] P.S.M. Rajesh, C. Delaroa, M. Gagné, J.E. Klemberg-Sapieha, F. Sirois, D. Therriault, Continuous and selective-area coating of silver on fiber-reinforced polymer composites for aerospace applications, Mater. Today Commun. 18 (2019) 206–212, https://doi.org/10.1016/j.mtcomm.2018.11.002.
[4] A. Baptista, G. Pinto, F.J.G. Silva, A.A. Ferreira, A.G. Pinto, V.F.C. Sousa, Wear Characterization of Chromium PVD Coatings on Polymeric Substrate for Automotive Optical Components, Coatings 11 (2021) 555, https://doi.org/10.3390/coatings11050555.
[5] A. Kausar, A review of filled and pristine polycarbonate blends and their applications, J. Plast. Film Sheeting 34 (1) (2018) 60–97, https://doi.org/10.1177/8756087917691088.
[6] E.V. Antonakou, D.S. Achilias, Recent Advances in Polycarbonate Recycling: A Review of Degradation Methods and Their Mechanisms, Waste Biomass Valori. 4 (1) (2013) 9–21, https://doi.org/10.1007/s12649-012-9159-x.
[7] M. Lindner, M. Schmid, Thickness Measurement Methods for Physical Vapor Deposited Aluminum Coatings in Packaging Applications: A Review, Coatings 7 (2017) 9, https://doi.org/10.3390/coatings7010009.
[8] M. Kharrazi Olsson, K. Macák, W. Graf, Reactive d.c. magnetron sputter deposited Al2O3 films: large-area coatings for industrial applications, Surf. Coat. Technol. 122 (2-3) (1999) 202–207, https://doi.org/10.1016/S0257-8972(99)00378-3.
[9] P.V. Kola, S. Daniels, D.C. Cameron, M.S.J. Hashmi, Magnetron sputtering of tin protective coatings for medical applications, J. Mater. Process. Technol. 56 (1–4) (1996) 422–430, https://doi.org/10.1016/0924-0136(95)01856-5.
[10] M. Hans, M. to Baben, D. Music, J. Ebenhöch, D. Primetzhofer, D. Kurapov, M. Arndt, H. Rudigier, J.M. Schneider, Effect of oxygen incorporation on the structure and elasticity of Ti-Al-O-N coatings synthesized by cathodic arc and high power pulsed magnetron sputtering, J. Appl. Phys. 116 (2014) 93515, https://doi.org/10.1063/1.4894776.
[11] J. Lackner, W. Waldhauser, A. Alamanou, C. Teichert, F. Schmied, L. Major, B. Major, Mechanisms for self-assembling topography formation in low-

temperature vacuum deposition of inorganic coatings on polymer surfaces, Bull. Pol. Acad. Sci. Tech. Sci. 58 (2010), https://doi.org/10.2478/v10175-010-0026-2.
[12] C. Massaro, Q.T. Le, J.J. Pireaux, XPS/AFM study of thermally evaporated aluminium/polycarbonate interface, Surf. Interface Anal. 21 (6–7) (1994) 425–429.
[13] C. Seidel, H. Kopf, B. Gotsmann, T. Vieth, H. Fuchs, K. Reihs, Ar plasma treated and Al metallised polycarbonate: A XPS, mass spectroscopy and SFM study, Appl. Surf. Sci. 150 (1-4) (1999) 19–33, https://doi.org/10.1016/S0169-4332(99)00012-4.
[14] C.S. Rastomjee, M. Keil, H. Sotobayashi, A.M. Bradshaw, C.L.A. Lamont, D. Gador, E. Umbach, Aluminium metallisation of argon and oxygen plasma-modified polycarbonate thin film surfaces, Appl. Surf. Sci. 136 (4) (1998) 280–297, https://doi.org/10.1016/S0169-4332(98)00348-1.
[15] A. Hooper, G.L. Fisher, K. Konstadinidis, D. Jung, H. Nguyen, R. Opila, R. W. Collins, N. Winograd, D.L. Allara, Chemical Effects of Methyl and Methyl Ester Groups on the Nucleation and Growth of Vapor-Deposited Aluminum Films, J. Am. Chem. Soc. 121 (35) (1999) 8052–8064, https://doi.org/10.1021/ja9835234.
[16] G.L. Fisher, A.V. Walker, A.E. Hooper, T.B. Tighe, K.B. Bahnck, H.T. Skriba, M. D. Reinard, B.C. Haynie, R.L. Opila, N. Winograd, D.L. Allara, Bond insertion, complexation, and penetration pathways of vapor-deposited aluminum atoms with HO- and CH(3)O-terminated organic monolayers, J. Am. Chem. Soc. 124 (19) (2002) 5528–5541, https://doi.org/10.1021/ja0123453.
[17] G.L. Fisher, A.E. Hooper, R.L. Opila, D.L. Allara, N. Winograd, The Interaction of Vapor-Deposited Al Atoms with CO 2 H Groups at the Surface of a Self-Assembled Alkanethiolate Monolayer on Gold †, J. Phys. Chem. B 104 (14) (2000) 3267–3273, https://doi.org/10.1021/jp993354p.
[18] K. Konstadinidis, R.L. Opila, J.A. Taylor, A.C. Miller, X-ray Photoelectron Study of Chemical Interactions at Ti/Polymer Interfaces, J. Adhes. 46 (1-4) (1994) 197–213, https://doi.org/10.1080/00218469408026660.
[19] F.S. Ohuchi, S.C. Freilich, Metal polyimide interface: A titanium reaction mechanism, J. Vac. Sci. Technol., A 4 (3) (1986) 1039–1045, https://doi.org/10.1116/1.573450.
[20] P. Bodö, J.-E. Sundgren, Adhesion of evaporated titanium to polyethylene: Effects of ion bombardment pretreatment, J. Vac. Sci. Technol., A 2 (4) (1984) 1498–1502, https://doi.org/10.1116/1.572460.
[21] G.M. Porta, J.D. Rancourt, L.T. Taylor, Interfacial interactions of titanium-coated polyester films, Chem. Mater. 3 (3) (1991) 423–428, https://doi.org/10.1021/cm00015a013.
[22] A. Lachkar, A. Selmani, E. Sacher, Metallization of polythiophenes II. Interaction of vapor-deposited Cr, V and Ti with poly(3-hexylthiophene) (P3HT), Synth. Met. 72 (1) (1995) 73–80, https://doi.org/10.1016/0379-6779(94)02319-T.
[23] K. Konstadinidis, P. Zhang, R.L. Opila, D.L. Allara, An in-situ X-ray photoelectron study of the interaction between vapor-deposited Ti atoms and functional groups at the surfaces of self-assembled monolayers, Surf. Sci. 338 (1-3) (1995) 300–312, https://doi.org/10.1016/0039-6028(95)80048-4.
[24] A. Calderone, R. Lazzaroni, J.L. Brédas, Q.T. Le, J.J. Pireaux, The aluminum/polyethylene terephthalate interface: A joint theoretical and experimental study, J. Chem. Phys. 102 (10) (1995) 4299–4307, https://doi.org/10.1063/1.469477.
[25] A.K. Chakraborty, H.T. Davis, M. Tirrell, A molecular orbital study of the interactions of acrylic polymers with aluminum: Implications for adhesion, J. Polym. Sci. A Polym. Chem. 28 (1990) 3185–3219, https://doi.org/10.1002/pola.1990.080281201.
[26] K. Anand, T. Duguet, J. Esvan, C. Lacaze-Dufaure, Chemical Interactions at the Al/Poly-Epoxy Interface Rationalized by DFT Calculations and a Comparative XPS Analysis, ACS Appl. Mater. Interfaces 12 (51) (2020) 57649–57665, https://doi.org/10.1021/acsami.0c1961610.1021/acsami.0c19616.s001.
[27] P. Keuter, S. Karimi Aghda, D. Music, P. Kümmerl, J.M. Schneider, Synthesis of Intermetallic (Mg1-x, Alx)2Ca by Combinatorial Sputtering, Materials 12 (2019) 3026, https://doi.org/10.3390/ma12183026.
[28] G. Beamson, D. Briggs, High resolution XPS of organic polymers: The Scienta ESCA300 database, Wiley, Chichester, 1992.
[29] M.C. Burrell, J.J. Chera, Polycarbonate Spin Cast Films by XPS, Surf. Sci. Spectra 6 (1) (1999) 1–4, https://doi.org/10.1116/1.1247900.
[30] W. Kohn, L.J. Sham, Self-Consistent Equations Including Exchange and Correlation Effects, Phys. Rev. 140 (4A) (1965) A1133–A1138, https://doi.org/10.1103/PhysRev.140.A1133.
[31] P. Hohenberg, W. Kohn, Inhomogeneous electron gas, Phys. Rev. B 136 (3B) (1964) B864–B871, https://doi.org/10.1103/PhysRev.136.B864.
[32] T. Ozaki, Variationally optimized atomic orbitals for large-scale electronic structures, Phys. Rev. B 67 (2003), 155108, https://doi.org/10.1103/PhysRevB.67.155108.
[33] T. Ozaki, H. Kino, Numerical atomic basis orbitals from H to Kr, Phys. Rev. B 69 (2004), 195113, https://doi.org/10.1103/PhysRevB.69.195113.
[34] T. Ozaki, H. Kino, Efficient projector expansion for the ab initio LCAO method, Phys. Rev. B 72 (2005) 45121, https://doi.org/10.1103/PhysRevB.72.045121.
[35] K. Lejaeghere, G. Bihlmayer, T. Björkman, P. Blaha, S. Blügel, V. Blum, D. Caliste, I. E. Castelli, S.J. Clark, A. Dal Corso, S. de Gironcoli, T. Deutsch, J.K. Dewhurst, I. Di Marco, C. Draxl, M. Dułak, O. Eriksson, J.A. Flores-Livas, K.F. Garrity, L. Genovese, P. Giannozzi, M. Giantomassi, S. Goedecker, X. Gonze, O. Grånäs, E.K.U. Gross, A. Gulans, F. Gygi, D.R. Hamann, P.J. Hasnip, N.A.W. Holzwarth, D. Iuşan, D. B. Jochym, F. Jollet, D. Jones, G. Kresse, K. Koepernik, E. Küçükbenli, Y. O. Kvashnin, I.L.M. Locht, S. Lubeck, M. Marsman, N. Marzari, U. Nitzsche, L. Nordström, T. Ozaki, L. Paulatto, C.J. Pickard, W. Poelmans, M.I.J. Probert, K. Refson, M. Richter, G.-M. Rignanese, S. Saha, M. Scheffler, M. Schlipf, K. Schwarz, S. Sharma, F. Tavazza, P. Thunström, A. Tkatchenko, M. Torrent, D. Vanderbilt, M.J. van Setten, V. van Speybroeck, J.M. Wills, J.R. Yates, G.-X. Zhang, S. Cottenier, Reproducibility in density functional theory calculations of solids, Science 351 (2016) 2–7, https://doi.org/10.1126/science.aad3000.
[36] S. Nosé, A unified formulation of the constant temperature molecular dynamics methods, J. Chem. Phys. 81 (1) (1984) 511–519, https://doi.org/10.1063/1.447334.
[37] T. Ozaki, C.-C. Lee, Absolute Binding Energies of Core Levels in Solids from First Principles, Phys. Rev. Lett. 118 (2017) 26401, https://doi.org/10.1103/PhysRevLett.118.026401.
[38] S. Grimme, J. Antony, S. Ehrlich, H. Krieg, A consistent and accurate ab initio parametrization of density functional dispersion correction (DFT-D) for the 94 elements H-Pu, J. Chem. Phys. 132 (15) (2010) 154104, https://doi.org/10.1063/1.3382344.
[39] G. Kresse, J. Hafner, Ab initio molecular dynamics for liquid metals, Phys. Rev. B 47 (1) (1993) 558–561, https://doi.org/10.1103/PhysRevB.47.558.
[40] G. Kresse, J. Furthmüller, Efficient iterative schemes for ab initio total-energy calculations using a plane-wave basis set, Phys. Rev. B 54 (16) (1996) 11169–11186, https://doi.org/10.1103/PhysRevB.54.11169.
[41] G. Kresse, D. Joubert, From ultrasoft pseudopotentials to the projector augmented-wave method, Phys. Rev. B 59 (3) (1999) 1758–1775, https://doi.org/10.1103/PhysRevB.59.1758.
[42] P.E. Blöchl, Projector augmented-wave method, Phys. Rev. B 50 (24) (1994) 17953–17979, https://doi.org/10.1103/PhysRevB.50.17953.
[43] J.P. Perdew, K. Burke, M. Ernzerhof, Generalized Gradient Approximation Made Simple, Phys. Rev. Lett. 77 (18) (1996) 3865–3868, https://doi.org/10.1103/PhysRevLett.77.3865.
[44] R. Dronskowski, P.E. Bloechl, Crystal orbital Hamilton populations (COHP): energy-resolved visualization of chemical bonding in solids based on density-functional calculations, J. Phys. Chem. 97 (33) (1993) 8617–8624, https://doi.org/10.1021/j100135a014.
[45] V.L. Deringer, A.L. Tchougréeff, R. Dronskowski, Crystal orbital Hamilton population (COHP) analysis as projected from plane-wave basis sets, J. Phys. Chem. A 115 (21) (2011) 5461–5466, https://doi.org/10.1021/jp202489s.
[46] S. Maintz, V.L. Deringer, A.L. Tchougréeff, R. Dronskowski, Analytic projection from plane-wave and PAW wavefunctions and application to chemical-bonding analysis in solids, J. Comput. Chem. 34 (29) (2013) 2557–2567, https://doi.org/10.1002/jcc.23424.
[47] R. Nelson, C. Ertural, J. George, V.L. Deringer, G. Hautier, R. Dronskowski, LOBSTER: Local orbital projections, atomic charges, and chemical-bonding analysis from projector-augmented-wave-based density-functional theory, J. Comput. Chem. 41 (2020) 1931–1940, https://doi.org/10.1002/jcc.26353.
[48] S. Maintz, V.L. Deringer, A.L. Tchougréeff, R. Dronskowski, LOBSTER: A tool to extract chemical bonding from plane-wave based DFT, J. Comput. Chem. 37 (11) (2016) 1030–1035, https://doi.org/10.1002/jcc.24300.
[49] P. Ondračka, D. Bogdanovski, NOMAD dataset: Polycarbonate interaction with Ti TiAl and Al surfaces. https://dx.doi.org/10.17172/NOMAD/2021.09.15-2, 2021.
[50] K. Momma, F. Izumi, VESTA 3 for three-dimensional visualization of crystal, volumetric and morphology data, J. Appl. Crystallogr. 44 (2011) 1272–1276, https://doi.org/10.1107/S0021889811038970.
[51] J.M. Lannon, Q. Meng, Analysis of Polycarbonate (PC) by XPS, Surf. Sci. Spectra 6 (2) (1999) 75–78, https://doi.org/10.1116/1.124790110.1116/1.1247901.N004610110.1116/1.1247901.N004610210.1116/1.1247901.N0046103.
[52] A. Ringenbach, Y. Jugnet, T.M. Duc, Interfacial chemistry in Al and Cu metallization of untreated and plasma treated polyethylene and polyethyleneterephthalate, J. Adhes. Sci. Technol. 9 (1995) 1209–1228, https://doi.org/10.1163/156856195X01003.
[53] M. Ohring, Materials science of thin films: Deposition and structure, second ed., Academic Press, San Diego, CA, 2002.
[54] S. Liu, K. Chang, D. Music, X. Chen, S. Mráz, D. Bogdanovski, M. Hans, D. Primetzhofer, J.M. Schneider, Stress-dependent prediction of metastable phase formation for magnetron-sputtered V1−xAlxN and Ti1−xAlxN thin films, Acta Mater. 196 (2020) 313–324, https://doi.org/10.1016/j.actamat.2020.06.044.